JCTC Journal of Chemical Theory and Computation

Article

pubs.acs.org/JCTC

What Dominates the Error in the CaO Diatomic Bond Energy Predicted by Various Approximate Exchange−Correlation Functionals?

Haoyu Yu and Donald G. Truhlar*

Department of Chemistry, Chemical Theory Center, and Supercomputing Institute, University of Minnesota, Minneapolis, Minnesota 55455-0431, United States

ABSTRACT: In order to understand what governs the accuracy of approximate exchange−correlation functionals for intrinsically multiconfigurational systems containing metal atoms, the properties of the ground electronic state of CaO have been studied in detail. We first applied the T1, TAE(T), B1, and M diagnostics to CaO and confirmed that CaO is an intrinsically multiconfigurational system. Then, we compared the bond dissociation energies (BDEs) of CaO as calculated by 49 exchange−correlation functionals, three exchange-only functionals, and the HF method. To analyze the error in the BDEs for the various functionals, we decomposed each calculated BDE into four components, in particular the ionization potential, the electron affinity, the atomic excitation energy of the metal cation to prepare the valence state, and the interaction energy between prepared states. We found that the dominant error occurs in the calculated atomic excitation energy of the cation. Third, we compared dipole moments of CaO as calculated by the 53 methods, and we analyzed the dipole moments in terms of partial atomic charges to understand the contribution of ionic bonding and how it is affected by errors in the calculated ionization potential of the metal atom. We then analyzed the dipole moment in terms of the charge distribution among orbitals, and we found that the orbital charge distribution does not correlate well with the difference between the calculated ionization potential and electron affinity. Fourth, we examined the potential curves and internuclear distance dependence of the orbital energies of the lowest-energy CaO singlet and triplet states to analyze the near-degeneracy aspect of the correlation energy. The most important conclusion is that the error tends to be dominated by the error in the relative energies of s and d orbitals in Ca^+, and the most popular density functionals predict this excitation energy poorly. Thus, even if they were to predict the BDE reasonably well, it would be due to cancellation of errors. The effect of the cation excitation energy can be understood in terms of an orbital picture, as follows. For most functionals the predicted cation excitation energy is too small, so it is too easy to delocalize charge from the oxygen 2p orbital to the Ca^+ d orbital; this overestimates the covalency and explains why most functionals overestimate the bond energy.

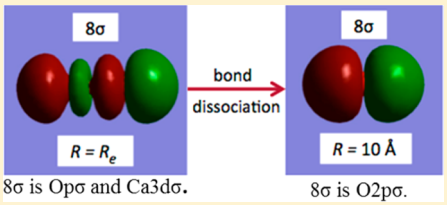

1. INTRODUCTION

It is well appreciated that accurate electronic structure calculations must include electron correlation. There are three types of electron correlation−dynamical correlation, left−right correlation, and angular correlation.[1−3] Dynamical correlation is associated with electrons avoiding each other to reduce their mutual Coulomb repulsion when they are close and with two electronic distributions correlating their fluctuating electric multipole moments for favorable long-range interaction when they are widely separated. Left−right correlation is a medium-range and long-range effect that accounts for nearly degenerate electronic configurations of a system due to building in diradical character in stretched bonds (including biradicals) and weak bonds;[4] left−right correlation is sometimes called static correlation. Angular correlation is mainly monatomic, and it can be especially large when it is associated with atomic near-degeneracies;[5] although it is necessarily short-range since it is monatomic, it is sometimes considered to be static[3] and sometimes dynamic.[1,2,6] Both left−right and angular correlation are near-degeneracy effects, and systems exhibiting significant near-degeneracy correlation effects may be classified as "intrinsically multiconfigurational", which is conveniently shortened to "multireference", an adjective that reminds us that wave function treatments of such systems must be based on a multiconfiguration reference function if they are to converge rapidly with respect to the level of excitations included in the correlated wave function.[7−9]

Although Kohn−Sham density functional theory[10] (KS-DFT) with the unknown universal exchange−correlation functional does not require a multiconfigurational representation of the density even for multireference systems, essentially all currently used exchange−correlation functionals are less accurate for the treatment of multireference systems than for the treatment of single-reference systems.[11] There is great interest in understanding this, especially because multireference character is frequently encountered in practically important systems containing transition metals. Ca is a main-group metal, but it comes just before the first transition metal (Sc) in the periodic table. Like many other compounds of group I and group II metals, Ca compounds often have multireference character.[12,13] In order to understand multireference systems

Received: February 1, 2014
Published: May 9, 2014

   dx.doi.org/10.1021/ct5000814 | J. Chem. Theory Comput. 2014, 10, 2291−2305

containing metal atoms, there is some advantage in starting with Ca compounds rather than transition metals because the ground state of Ca is a closed-shell singlet with no occupied d orbitals. For this reason, we embarked on a study of CaO to try to understand which aspects of approximate exchange−correlation functionals make them more or less accurate for metal compounds with multireference character. There are two other reasons, besides the absence of d electrons in the ground state of the metal atom, that make CaO easier to understand than transition metal complexes. First, CaO has fewer electrons than a typical transition metal compound. Second, CaO has only one chemical bond. Previously, CaO has been studied by wave function theory with the main focus being the dipole moment and low-lying excited state.[14,15] Here, we apply density functional theory and mainly focus on the bond energy and dipole moment. We also compare our calculated results to the experimental[16] Rydberg−Klein−Rees potential energy curve.

The motivation of this research is to better understand multireference character and the sources of the largest errors of approximate exchange−correlation functionals for metal−ligand bonds. Once we understand this issue for CaO, we hope to be able to apply what we learn to transition metals and other multireference systems.

The present work is organized as follows. The second section gives computational details of our work. Section 3 presents multireference diagnostics that confirm the multireference character of CaO; section 4 includes our calculations and results. In section 5, we discuss the bond dissociation energy and its components, the dipole moment, the potential curve, and the orbital energies. The conclusions are in section 6.

2. COMPUTATIONAL DETAILS

All calculations of CaO (except the potential energy curves and orbital energies as functions of internuclear distance R) are carried out at the experimental equilibrium value of R, which is R_e = 1.821 Å.[17] We always set the molecule CaO on the z-axis. We use the aug-cc-pCVQZ basis set for O and cc-pCVQZ for Ca for all the calculations in this paper.[18,19]

All calculations are nonrelativistic. For the M06-L density functional, we checked that the calculated bond energy increases from 113.32 to 114.39 kcal/mol (an 0.9% increase) when scalar relativistic effects are included by the second-order Douglas−Kroll−Hess[20−23] approximation. We also considered the spin−orbit effect of O, which decreases the bond energy of CaO by −0.22 kcal/mol.[24] If we consider scalar relativistic effects and spin−orbit effect together, the calculated BDE of CaO by M06-L should be changed from 113.32 to 114.17 kcal/mol (an 0.7% increase). This is small enough that it does not affect our conclusions, so all calculations presented in the rest of this paper are nonrelativistic without spin−orbit effects.

There are two kinds of broken-symmetry aspects to our calculations. First, we use unrestricted Hartree−Fock theory or spin-polarized KS-DFT (the latter is sometimes called unrestricted KS); these treatments involve different spatial orbitals for α and β electrons so the Kohn−Sham determinant is not an eigenfunction of the multielectron operator S^2, where S is total electron spin. After the unrestricted Hartree−Fock or spin-polarized KS-DFT calculation has apparently converged, the solution is analyzed for stability with respect to further symmetry breaking by using the stable=opt keyword of *Gaussian 09*[25] to search for variations that lower the energy. The SCF optimization is then carried to convergence to a stable solution. None of the CaO calculations break symmetry at R = R_e, that is, the restricted Hartree−Fock solution is stable to breaking either spin symmetry (which would yield a so-called unrestricted solution) or spatial symmetry. However, at large R, the oxygen atom becomes a spin-polarized triplet, and we also find spin polarization in the potential-energy-curve and orbital-energy calculations at large R; that is, the restricted solution is unstable with restrict to allowing it to be unrestricted.

We applied four multireference diagnostics to CaO at its equilibrium geometry. The T_1, TAE(T), and B_1 diagnostics[26−30] were calculated by using *Gaussian 09*; the M diagnostic[29] was calculated by using *Molpro*.[31] CASSCF calculations[32] with an active space of 8 electrons in 10 orbitals are employed to calculate the M diagnostic. All the diagnostics are explained in the following section.

A benchmark value for the dipole moment of CaO was calculated by the CCSDT method[33] with *NWChem*.[34]

3. DIAGNOSTICS OF CAO

First, we apply the T_1 diagnostic to our system. Lee and Taylor proposed that the norm of the vector of single-excitation amplitudes (t_1 amplitudes) in a closed-shell coupled-cluster singles and doubles (CCSD) wave function could be used as a diagnostic for the prediction of the reliability of results obtained from a single-reference-based electron correlation procedure.[26] The T_1 diagnostic is

$$T_1 = \frac{\| t_1 \|}{N_{\text{elec}}^{1/2}} \tag{1}$$

where N_{elec} is the number of the electrons of a system, and t_1 is the vector of single-excitation amplitudes in a CCSD calculation. If T_1 is smaller than 0.02, the system under consideration is considered to be a single-reference system; if T_1 is larger than 0.02, the system is a multireference system. Although it is well-known that this diagnostic is sometimes small for multireference systems (and so it is not a reliable diagnostic in general), when it large it is a reasonably reliable indicator of multireference character. We calculated T_1 = 0.037 for CaO. Therefore, CaO is a multireference system according to the T_1 diagnostic.

Second, we apply the %TAE[T] diagnostic to CaO; it is defined as[27]

$$\%\text{TAE[T]} = 100\left(\frac{\text{AE[CCSD(T)} - \text{AE[CCSD]]}}{\text{AE[CCSD(T)]}}\right) \tag{2}$$

where AE[CCSD] is the atomization energy of the system calculated with the coupled cluster method including single and double excitations and AE[CCSD(T)] is the atomization energy of the system calculated with CCSD plus a quasiperturbative treatment of connected triple excitations. If %TAE[T] is smaller than 2%, the system under consideration is considered to be a single-reference system; if it is larger than 2% and smaller than 10%, the system is a moderate multireference system; and if it is larger than 10%, then the system is a multireference system.[27] We calculated that %TAE(T) = 11.7%. Therefore, CaO is a multireference system according to the %TAE(T) diagnostic.

Third, we apply the B_1 diagnostic[28−30] to the CaO bond. This diagnostic is defined for a single bond as

$$B_1 = [D_e(\text{BLYP}) - D_e(\text{B1LYP//BLYP})] \tag{3}$$

where D_e is the energy required to break the bond, BLYP is the combination of the Becke (B) 1988 local exchange functional

Table 1. List of Density Functionals Used in the Present Study[a]

name	ref	X^b	τ^c
B1LYP	37	25	no
B3LYP	45	20	no
B3LYP*	46	15	no
B88X[d]	35	0	no
B97-1	47	21	no
B97-3	48	26.93	no
BLYP	35, 36	0	no
BP86	35, 49	0	no
BPW91	35, 50	0	no
CAM-B3LYP	51	19−65	no
GVWN5[e]	52−54	0	no
HF[d]	55−57	100	no
HFLYP	58	100	no
HSE	59, 60	0−25	no
M05	61	28	yes
M05-2X	62	56	yes
M06	63	27	yes
M06-2X	63	54	yes
M06-L	64	0	yes
M08-HX	65	52.23	yes
M08-SO	65	56.79	yes
M11	66	42.8−100	yes
M11-L	67	0	yes
MN12-L	68	0	yes
MN12-SX	69	25−0	yes
MOHLYP	70	0	no
MPW1B95	71	31	yes
MPWB1K	71	44	yes
MPWLYP1M	70	5	no
mPWPW	50, 72	0	no
N12	73	0	no
N12-SX	69	5−60	no
O3LYP	74	11.61	no
OHLYP	36, 2	0	no
OLYP	36, 2	0	no
OptX[d]	2, 74	0	no
OreLYP	2, 36, 75	0	no
PBE	76	0	no
PBE0	77	25	no
PBEsol	78	0	no
PBEX[d]	76, 79	0	no
PW6B95	80	28	yes
PW91	50	0	no
revTPSS	81	0	yes
revTPSSVP86	49, 54, 81	0	yes
SOGGA	82	0	no
SOGGA11	83	0	no
SOGGA11-X	84	35.42	no
TPSSh	85	10	yes
τ-HCTHhyb	86	15	yes
ωB97	87	100	no
ωB97X	87	15.77−100	no
ωB97X-D	88	22.2−100	no

[a]For completeness the table also includes the Hartree−Fock method. [b]Nominal percentage of nonlocal HF exchange. [c]Noninteracting kinetic energy density. [d]This method has no correlation functional. [e]Gáspár for exchange and VWN5 for correlation; this is an example of the local spin density approximation (LSDA, which becomes LDA for closed-shell singlets), and it has the keyword SVWN5 in the *Gaussian 09* program. Note that the G exchange functional was also used by Kohn and Sham and is sometimes called GKS; it is 2/3 times the value derived by Slater. The normalization used by Gáspár, Kohn, and Sham was also used earlier by Bloch and Dirac.

(B88X)[35] and the Lee−Yang−Parr (LYP) correlation functional,[36] B1LYP stands for an exchange−correlation functional in which the Hartree−Fock exchange and B88X exchange are mixed in the ratio 1/4 and in which the correlation functional is LYP,[37] and B1LYP//BLYP denotes a B1LYP calculation using the BLYP equilibrium geometries for the molecule and the fragments. The B_1 diagnostic is based on the realization that the Hartree−Fock exchange approximation fails badly for multireference systems because it introduces static correlation error. The criterion that has been adopted[28] is that if B_1 is larger than 10 kcal/mol then the system is classified as a multireference system; otherwise, it is classified as a single-reference system. (Sometimes the B_1 diagnostic is better interpreted as a diagnostic of a "difficult case," but here, we use it as a multireference diagnostic.) We calculated B_1 = 21.7 kcal/mol for CaO; therefore, CaO is a multireference system according to the B_1 diagnostic.

Finally, we apply the M diagnostic to CaO. For a system such as CaO, at the equilibrium geometry with no singly occupied molecular orbitals in the dominant configuration, the M diagnostic is defined as[29]

$$M = \frac{1}{2}(2 - n(\mathrm{MCDONO}) + n(\mathrm{MCUNO})) \quad (4)$$

where $n(j)$ is a natural orbital occupation number (which we here evaluate, as usual, as an eigenvalue of the first-order density matrix of a CASSCF wave function), and n(MCDONO) and n(MCUNO) are respectively the natural orbital occupation numbers of the most correlated doubly occupied natural orbital (MCDONO) and the most correlating unoccupied natural orbital (MCUNO). If M is larger than 0.04, then the system is considered to be a multireference system; otherwise, it is considered to be a single-reference system.[29]

To calculate the M diagnostic of CaO, we carried out a complete active space self-consistent field calculations at the equilibrium geometry with an active space of eight electrons in ten orbitals (2s and 2p orbitals from oxygen, 4s and 3d orbitals from calcium). The natural orbital occupation numbers are 1.9828, 1.9585, 1.9551, 1.9551, 0.0434, 0.0434, 0.0414, 0.0148, 0.0028, and 0.0028, listed in order of decreasing occupation number. The symmetry of the ground state is $^1\Sigma_g^+$. There are 16 electrons in σ orbitals and 12 electrons in π orbitals. This calculation yields the following order of the orbitals in the active space, listed in order of increasing energy, identified by the dominant atomic orbital or orbitals and with the molecular orbital ordering in each symmetry in parentheses: O2s(7σ), O2pσ(8σ), O2p$_x$Ca3dπ($3\pi_x$), Op$_y$Ca3dπ($3\pi_y$), Ca4s(9σ), O2pπ($4\pi_y$), O2pπ($4\pi_x$), Ca3dσ(10σ), Ca3dδ($1\delta_x2_{-y}2$), Ca3dδ-($1\delta_{xy}$) orbitals. (When two atomic orbitals are listed, the one listed first makes the greater contribution.) The HOMO orbital of a Hartree−Fock calculation would be O 2pCa3dπ(3π), and the LUMO orbital would be Ca4s(9σ). In the present case, the MCDONO turns out to be the HOMO with 1.955 electrons,

dx.doi.org/10.1021/ct5000814 | J. Chem. Theory Comput. 2014, 10, 2291−2305

and the MCUNO turns out to be the LUMO with 0.043 electrons; consequently, M is 0.044, and CaO is a multireference system according to the M diagnostic.

In summary, CaO is a multireference system according to all four diagnostics.

4. CALCULATIONS AND RESULTS

We applied 49 exchange−correlation functionals, three exchange-only functionals, and Hartree−Fock theory to calculate the bond dissociation energy (BDE) of CaO. These methods are listed in Table 1, which also gives the original reference or references for each of them, the percentage X of Hartree−Fock exchange, and whether or not the functional includes kinetic energy density (τ). All density functional calculations were carried out using *Gaussian 09* and MN-GFM 6.4.[38]

One noteworthy aspect of Table 1 is that it includes a relatively recent functional, in particular the OreLYP functional, which is a reoptimized LYP functional for correlation (reLYP)[75] and OptX for exchange.[2] The reLYP correlation function of Thakkar is a version of the LYP correlation functional that is designed to be more accurate for atoms with atomic number larger than 19 without unreasonably degrading accuracy for lighter atoms; it is very interesting to apply it to Ca because Ca has $Z = 20$.

The set of functionals studied also contains Becke's very widely used 1988 generalized gradient approximation functional (commonly called B, B88, or B88X),[35] as well as two other exchange-only functionals (OptX and PBEX); the reader may compare these results to the Hartree−Fock results to help sort out the effects of changing the treatment of exchange in the absence of correlation. The density functional revTPSSVP86 is first introduced in the present paper; it is the combination of revTPSS[81] exchange functional and VP86 correlation functional which is a combination of VWN5[54] correlation functional and the P86[49] correlation functional.

The BDE of CaO is defined as

$$\mathrm{BDE} = D_e(\mathrm{CaO}) = E(\mathrm{Ca}) + E(\mathrm{O}) - E(\mathrm{CaO}) \quad (1)$$

where E is electronic energy (which includes nuclear repulsion when present). The calculated BDEs are given in Table 2, where signed errors (SEs) are given with respect to the experimental[39,40] equilibrium bond energy D_e. The experimental value of D_e is taken as the experimental value[39] of D_0, which is 95.1 kcal/mol, plus the zero point energy, which is computed in the harmonic approximation from the experimental frequency;[40] this yields D_e = 96.1 kcal/mol.

Table 2 also contains charges calculated by dividing the dipole moment by the experimental bond distance. Table 2 shows that the charge distribution is approximately Ca^{1+} and O^{1-}. Furthermore, natural bond orbital (NBO) analysis[41] of CaO shows that the single valence electron of Ca^{1+} is in an orbital with predominantly d character. Therefore, we think of the bond forming process of CaO as follows: We begin with neutral Ca and O atoms. Then Ca is ionized by losing an electron, the cost for which is the ionization potential (IP) of Ca. Next O attaches the electron, the energy release for which is the electron affinity (EA) of O. Then $Ca^+(s)$ is excited to $Ca^+(d)$, the cost for which is the first excitation energy (EE) of Ca^+. Now the reagents are properly prepared in their valence states, and they interact to form a bond. We call the energy released when CaO is formed from $Ca^+(d)$ and O^- the interaction energy (IE). These steps and their associated energies are shown in Figure 1. We conclude from this hypothetical bond forming process that

$$\mathrm{BDE} = \mathrm{EA} - \mathrm{IP} - \mathrm{EE} + \mathrm{IE} \quad (2)$$

Table 2. Bond Dissociation Energy of CaO, Signed Error (kcal/mol), and Charge on Ca in CaO of CaO (Calculated from the Dipole Moment), Sorted in Order of Increasing Magnitude of the Error

name	BDE(CaO)	SE	q (Ca)
MN12-L	96.2	0.1	0.99
B1LYP	97.2	1.1	1.12
M08-HX	94.7	−1.4	1.02
MN12-SX	98.0	1.9	1.06
M05-2X	93.6	−2.5	1.14
SOGGA11-X	92.6	−3.5	1.10
M11-L	91.9	−4.2	0.95
MPWB1K	91.6	−4.5	1.11
B97-3	100.8	4.7	1.04
M05	101.0	4.9	1.04
OHLYP	101.4	5.3	0.89
ωB97X	101.4	5.3	1.15
MPW1B95	101.5	5.4	1.05
M06	102.0	5.9	1.12
M08-SO	90.1	−6.0	1.04
CAM-B3LYP	102.3	6.2	1.12
ωB97	102.5	6.4	1.09
M06-2X	89.4	−6.7	1.17
HSE	102.8	6.7	1.03
PW6B95	102.8	6.7	1.04
PBE0	103.0	6.9	1.04
ωB97X-D	103.3	7.2	1.11
B3LYP	104.5	8.4	1.01
B97-1	106.4	10.3	0.85
PBEX	85.3	−10.8	1.02
OptX	83.4	−12.7	0.86
N12-SX	109.5	13.4	1.04
B3LYP*	110.0	13.9	0.98
M11	110.4	14.3	1.15
TPSSh	110.5	14.4	0.99
O3LYP	110.8	14.7	0.96
MOHLYP	111.8	15.7	0.89
τ-HTCHhyb	113.4	17.3	1.01
M06-L	114.4	18.3	0.98
revTPSS	115.3	19.2	0.94
MPWLYP1M	115.4	19.3	0.92
revTPSSVP86	116.8	20.7	0.94
OreLYP	116.8	20.7	0.90
N12	117.3	21.2	0.91
BLYP	118.6	22.5	0.90
OLYP	118.9	22.8	0.91
SOGGA11	123.0	26.9	0.92
BPW91	123.5	27.4	0.92
PBE	124.3	28.2	0.92
BP86	124.6	28.5	0.92
mPWPW	124.9	28.8	0.92
PW91	126.3	30.2	0.92
SOGGA	132.4	36.3	0.92
PBEsol	132.8	36.7	0.92
HFLYP	48.3	−47.8	1.29
GVWN5	146.2	50.1	0.93
HF	12.0	−84.1	1.29
B88X	−13.0	−109.1	1.48

dx.doi.org/10.1021/ct5000814 | J. Chem. Theory Comput. 2014, 10, 2291−2305

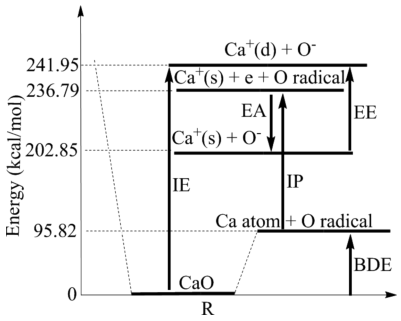

Figure 1. Decomposition of the bond dissociation energy of CaO.

We believe that a good functional should not only predict BDE accurately, but it should also predict the components EA, IP, ΔE, and IE; otherwise one might be concerned that a good value for the BDE arises from a fortuitous cancellation of errors.

With this theoretical framework in place, we calculated EA, IP, EE, and IE for all 53 methods, and the results are given in Tables 3, 4, and 5, which also show the errors of these calculated properties. The errors in Tables 3 and 4 are based on the experimental ionization potential of Ca atom of 141.0 kcal/mol,[42] the experimental electron affinity of O atom of 33.9 kcal/mol,[43] and the experimental electronic excitation energy of Ca^+ of 39.1 kcal/mol.[44] The last two columns of Table 4 will be explained in the following.

5. ANALYSIS AND DISCUSSION

5.1. Statistical Analysis. It is interesting to see which component of the BDE dominates the error. To try to avoid conclusions overly biased by outliers, fortuitously successful results, or the less accurate functionals, we consider the tenth smallest unsigned error for each property; we find (from the tables) 1.0 kcal/mol for IP, 1.3 kcal/mol for EA, 1.6 kcal/mol for IE, and 10.9 kcal/mol for EE. This shows very dramatically that EE is the hardest of the four quantities for KS-DFT to calculate, and it tends to dominate the error in BDE. Table 4 shows that all of the methods except HF give a smaller EE than the experimental value (39.1 kcal/mol). So, it is important to understand the origin of the systematic underestimation of EE by KS-DFT.

One attempt to understand the excitation energy, which is a many-electron quantity, is to relate it to a one-electron property; for example, in the orbital energy gap $\varepsilon_2-\varepsilon_1$ or the orbital energy gap $\varepsilon_3-\varepsilon_1$, where ε_1 is the orbital energy of the occupied 4s orbital of the ground state of Ca^+, ε_2 is the orbital energy of the unoccupied $3d\pi_x$ orbital of the ground state of Ca^+, and ε_3 is the orbital energy of the occupied $3d\pi_x$ orbital of the first excited state of Ca^+. Table 4 gives both of these gaps. We find that the magnitude of EE does not correlate with either of these orbital energy differences (nor do they correlate well with each other). This shows that the excitation energy can only be understood in a many-electron framework, which is consistent with an especially high angular-correlation contribution due to the near degeneracy of the 4s and 3d electrons.

Since all 49 exchange–correlation functionals and all three exchange-only functionals underestimate the excitation energy, whereas HF overestimates it, we consider successive modifications to a sequence of calculations starting with HF. Table 4 shows that adding LYP correlation to HF, as in HFLYP, lowers the excitation energy from 43 to 36 kcal/mol; these values straddle the accurate value of 39 kcal/mol.

Table 3. Ionization Potentials of Ca and Electron Affinities of O Radical and Their Signed Errors (in kcal/mol), Sorted in Each Case in Order of Increasing Magnitude of the Error

name	IP (Ca)	SE	name	EA (O)	SE
MPWLYP1M	140.8	−0.1	ωB97X-D	33.8	−0.2
M06-L	140.8	−0.1	PW6B95	33.8	−0.2
SOGGA11	141.1	0.1	B97−3	33.8	−0.2
PW91	140.6	−0.4	B97−1	34.1	0.2
OreLYP	141.6	0.6	M08-HX	34.2	0.3
B3LYP	141.6	0.6	O3LYP	34.4	0.5
B3LYP*	141.6	0.7	B1LYP	33.4	−0.5
M05	141.7	0.7	revTPSSVP86	34.8	0.9
CAM-B3LYP	140.2	−0.8	M11	34.9	1.0
PBE	139.9	−1.0	M05-2X	32.6	−1.3
ωB97X-D	139.8	−1.2	MOHLYP	35.4	1.5
N12-SX	139.8	−1.2	SOGGA11-X	32.5	−1.5
B97−3	142.2	1.3	M06-2X	32.5	−1.5
BLYP	139.6	−1.4	revTPSS	32.4	−1.6
revTPSSVP86	139.4	−1.6	M06	32.4	−1.6
BP86	142.6	1.6	OLYP	35.7	1.8
B97−1	142.7	1.7	HSE	32.1	−1.8
PW6B95	139.2	−1.8	PBE0	32.0	−2.0
mPWPW	139.1	−1.8	τ-HTCHhyb	36.1	2.1
PBEsol	138.8	−2.1	N12-SX	31.7	−2.2
GVWN5	143.2	2.3	TPSSh	31.6	−2.3
B1LYP	138.4	−2.5	M05	31.6	−2.4
M06	143.6	2.7	MN12-SX	31.4	−2.5
HSE	138.3	−2.7	M08-SO	36.5	2.5
revTPSS	138.2	−2.8	SOGGA	37.2	3.3
PBE0	138.2	−2.8	MPW1B95	30.5	−3.4
M08-HX	144.1	3.1	OreLYP	37.4	3.5
M06-2X	144.2	3.2	CAM-B3LYP	38.1	4.2
O3LYP	137.7	−3.2	M11-L	29.7	−4.2
BPW91	137.6	−3.4	M06-L	29.4	−4.5
TPSSh	137.5	−3.5	ωB97	29.4	−4.5
ωB97X	137.0	−3.9	B3LYP	38.8	4.9
MOHLYP	136.9	−4.0	ωB97X	39.2	5.3
M08-SO	145.1	4.1	BPW91	39.5	5.6
MPW1B95	136.9	−4.1	N12	28.2	−5.8
SOGGA	136.4	−4.5	PBEsol	39.9	6.0
OLYP	136.2	−4.7	B3LYP*	40.3	6.3
MPWB1K	136.1	−4.9	mPWPW	40.9	6.9
M11	136.0	−5.0	PBE	40.9	7.0
SOGGA11-X	146.4	5.5	MPWLYP1M	41.5	7.6
τ-HTCHhyb	146.5	5.5	MPWB1K	26.3	−7.6
HFLYP	135.3	−5.7	BLYP	42.1	8.1
ωB97	147.8	6.9	PW91	42.1	8.2
M05-2X	148.7	7.7	MN12-L	25.5	−8.4
MN12-L	149.3	8.3	BP86	44.0	10.0
N12	131.4	−9.6	OHLYP	23.8	−10.1
M11-L	151.1	10.2	SOGGA11	44.1	10.2
MN12-SX	151.2	10.2	PBEX	20.5	−13.4
OHLYP	127.8	−13.1	GVWN5	47.5	13.6
PBEX	124.9	−16.0	B88X	18.4	−15.5
B88X	122.1	−18.9	HFLYP	12.2	−21.8
OptX	119.7	−21.3	OptX	12.0	−21.9
HF	118.1	−22.9	HF	−13.2	−47.1

Similarly, adding LYP correlation energy to a local exchange functional, as in going from B88X to BLYP or from OptX to OLYP, also lowers the calculated excitation energy. Thus, HF exchange favors the s orbital relative to the d orbital and

dx.doi.org/10.1021/ct5000814 | J. Chem. Theory Comput. 2014, 10, 2291−2305

Table 4. Excitation Energy of Ca^+(s) and Its Signed Error, Sorted in Order of Increasing Magnitude of the Error (kcal/mol) and Compared to Orbital Energy Gap Between the Ground-State Ca^+ 4s Orbital and Ground-State Ca^+ $3d\pi_x$ Orbital ($\varepsilon_2-\varepsilon_1$) and Compared to the Orbital Energy Gap between the Ground-State Ca^+ 4s Orbital and the First-Excited State Ca^+ $3d\pi_x$ Orbital ($\varepsilon_3-\varepsilon_1$)

name	EE Ca^+(s)	SE	$\varepsilon_2-\varepsilon_1$	$\varepsilon_3-\varepsilon_1$
HFLYP	35.7	−3.4	175.6	24.3
HF	43.4	4.3	170.4	33.6
PBEX	34.6	−4.5	27.5	68.6
M06-2X	32.7	−6.4	126.0	56.7
B88X	32.2	−6.9	27.8	68.0
M08-SO	31.4	−7.7	116.2	47.5
MPWB1K	29.4	−9.7	101.9	52.6
ωB97X	28.8	−10.3	162.3	46.4
B1LYP	28.7	−10.4	68.1	57.3
CAM-B3LYP	28.2	−10.9	121.7	51.4
MPW1B95	28.2	−10.9	77.0	57.5
SOGGA11	28.1	−11.0	11.1	65.4
OptX	27.9	−11.2	26.0	65.7
PW6B95	27.7	−11.4	70.6	57.9
B3LYP	27.5	−11.6	57.4	59.2
M05	27.4	−11.7	63.9	54.5
MPWLYP1M	27.3	−11.8	27.4	64.0
B3LYP*	27.2	−11.9	47.4	61.3
M08-HX	27.1	−12.0	113.4	46.9
M05-2X	26.9	−12.2	124.7	50.1
HSE	26.7	−12.4	49.0	59.0
PBE0	26.4	−12.7	66.7	57.9
GVWN5	26.3	−12.8	14.4	71.3
BLYP	25.9	−13.2	17.4	65.1
SOGGA11-X	25.7	−13.4	93.0	50.7
B97-3	25.4	−13.7	70.5	57.1
M06	25.0	−14.1	64.3	61.7
SOGGA	24.6	−14.5	16.5	68.5
OHLYP	24.5	−14.6	21.1	63.0
MOHLYP	24.5	−14.6	18.5	64.9
PBE	24.3	−14.8	16.0	66.2
PBEsol	24.1	−15.0	16.4	68.7
B97-1	23.9	−15.2	57.5	58.2
ωB97X-D	23.8	−15.3	146.2	52.5
PW91	23.7	−15.4	15.5	66.5
BP86	23.1	−16.0	17.1	67.4
N12	22.8	−16.3	8.5	56.2
O3LYP	22.8	−16.3	38.8	59.6
mPWPW	22.8	−16.3	16.0	66.2
revTPSSVP86	22.5	−16.6	24.2	67.8
BPW91	21.9	−17.2	16.4	65.8
TPSSh	21.9	−17.2	38.9	61.3
revTPSS	21.5	−17.6	22.1	66.1
OLYP	21.3	−17.8	18.4	58.6
M11	21.0	−18.1	160.2	39.4
OreLYP	20.8	−18.3	17.8	58.5
N12-SX	20.5	−18.6	41.0	52.0
M11-L	19.3	−19.8	19.8	43.5
τ-HTCHhyb	18.8	−20.3	47.0	54.4
MN12-SX	17.2	−21.9	38.9	37.3
M06-L	16.4	−22.7	25.2	67.6
ωB97	16.3	−22.8	166.6	39.9
MN12-L	10.5	−28.6	34.1	39.3

Table 5. Interaction Energies (IE) and Their Signed Errors (SE), Sorted in Order of Increasing Magnitude of the Error (kcal/mol), Followed by the Average Unsigned Errors (AUE) of BDE, IP, EA, EE, and IE (kcal/mol), with the Functionals Arranged in Order of Increasing AUE[a]

name	IE (CaO)	SE	name	AUE (CaO)
M06-L	242.2	−0.1	M05	4.7
τ-HTCHhyb	242.6	0.3	B1LYP	5.2
BLYP	242.0	−0.3	M06-2X	5.2
MPWLYP1M	242.0	−0.3	PW6B95	5.3
revTPSS	242.7	0.4	M08-HX	5.5
OreLYP	241.8	−0.5	B97-3	5.5
N12	243.3	1.0	M06	5.7
BPW91	243.5	1.2	M05-2X	5.9
OLYP	240.8	−1.5	MPW1B95	6.0
revTPSSVP86	243.9	1.6	HSE	6.1
B97-1	238.9	−3.4	B97-1	6.2
mPWPW	246.0	3.7	PBE0	6.2
B3LYP*	238.6	−3.7	CAM-B3LYP	6.4
M05	238.5	−3.8	M08-SO	6.5
M06	238.3	−4.0	B3LYP	6.6
BP86	246.3	4.0	ωB97X-D	6.6
TPSSh	238.2	−4.1	SOGGA11-X	6.8
N12-SX	238.1	−4.2	B3LYP*	7.3
MOHLYP	237.8	−4.5	MPWB1K	7.6
ωB97	237.2	−5.1	ωB97X	7.8
PBE	247.6	5.3	MPWLYP1M	7.8
O3LYP	236.9	−5.4	N12-SX	7.9
SOGGA11	248.1	5.8	O3LYP	8.0
M05-2X	236.5	−5.8	MOHLYP	8.1
PW91	248.5	6.2	revTPSSVP86	8.3
PW6B95	236.0	−6.3	TPSSh	8.3
MPW1B95	235.9	−6.4	revTPSS	8.3
PBE0	235.7	−6.6	OreLYP	8.7
HSE	235.6	−6.7	MN12-SX	8.8
MN12-SX	235.0	−7.3	τ-HTCHhyb	9.1
B3LYP	234.9	−7.4	BLYP	9.1
B97−3	234.7	−7.6	ωB97	9.1
M06-2X	233.9	−8.4	M06-L	9.1
ωB97X-D	233.1	−9.2	M11	9.6
M11-L	232.6	−9.7	M11-L	9.6
M11	232.6	−9.7	OLYP	9.7
CAM-B3LYP	232.5	−9.8	N12	10.8
SOGGA11-X	232.2	−10.1	SOGGA11	10.8
M08-HX	231.7	−10.6	BPW91	11.0
B1LYP	230.9	−11.4	OHLYP	11.1
MPWB1K	230.8	−11.5	PBE	11.3
MN12-L	230.4	−11.9	MN12-L	11.5
M08-SO	230.1	−12.2	mPWPW	11.5
OHLYP	230.0	−12.3	BP86	12.0
PBEsol	255.8	13.5	PW91	12.1
SOGGA	256.3	14.0	PBEX	12.5
ωB97X	228.1	−14.2	SOGGA	14.5
PBEX	224.4	−17.9	PBEsol	14.7
OptX	219.0	−23.3	OptX	18.1
GVWN5	268.3	26.0	GVWN5	21.0
HFLYP	207.1	−35.2	HFLYP	22.8
HF	186.6	−55.7	HF	42.8
B88X	122.9	−119.4	B88X	54.0

[a]Experimental value of IE of CaO is the sum of the experimental values of IP, −EA, EE, and BDE.

dx.doi.org/10.1021/ct5000814 | J. Chem. Theory Comput. 2014, 10, 2291−2305

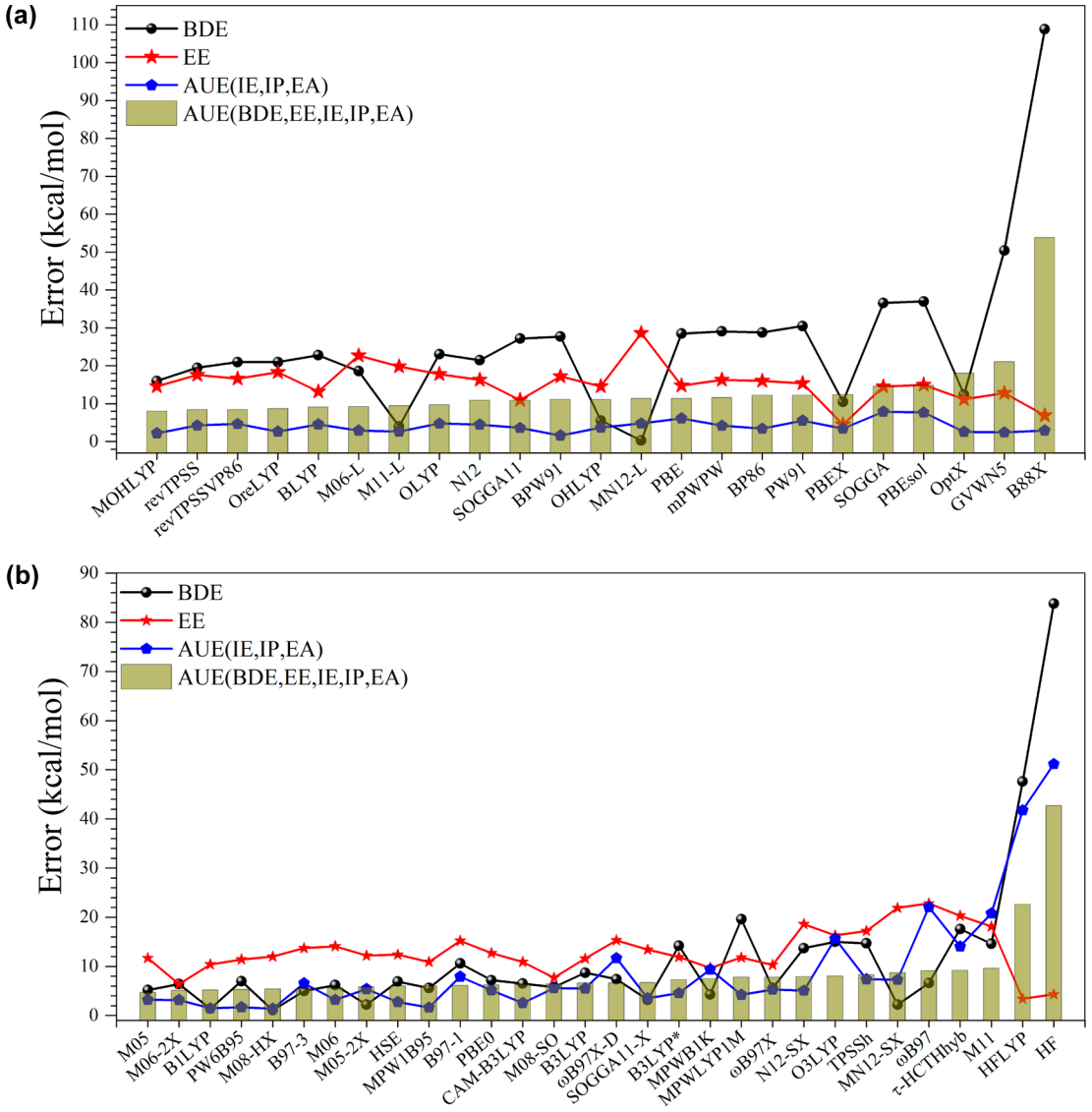

Figure 2. Unsigned errors (UEs) for local functionals (a) and hybrid functionals and the Hartree−Fock method. The black results are the UE in the bond dissociation energy, the red results are the UE in the Ca^+ excitation energy, the blue results are average of the UEs in the interaction energy, ionization potential, and the electron affinity, and the green results are the average of the UEs in the bond dissociation energy, the Ca^+ excitation energy, the interaction energy, ionization potential, and the electron affinity.

correlation favors the d orbital. Of the exchange-correlation functionals that include both exchange and correlation, the best balance between s and d orbital is achieved by M06-2X with an error of only −6.4 kcal/mol, followed by M08-SO (−7.7 kcal/mol), MPWB1K (−9.7 kcal/mol), ωB97X (−10.3 kcal/mol), and B1LYP (−10.4 kcal/mol).

Another informative way to look at the results in Table 4 is to compare the four exchange-only KS-DFT calcuations to the HF calculation, with the only difference being that exchange-only KS-DFT replaces HF nonlocal exchange by local exchange. The three local-exchange calculations give EE values (in kcal/mol) of 34.6 (PBEX), 32.2 (B88X), 27.9 (OptX); of these, OptX is the farthest from HF (43.4), which is curious, since OptX contains three parameters explicitly optimized against atomic exchange energies of 18 atoms, whereas B88X was optimized with a single parameter against the exchange energies of six noble-gas atoms. A related comparison is obtained by considering the sequence HF, OptX, OHLYP, OLYP, OreLYP, where OHLYP is a functional similar to OLYP (which is OptX exchange plus LYP correlation), except with only half of the correlation energy (HLYP denotes "half LYP"), as motivated by the fact that the LYP functional is well-known to overestimate correlation energy. The signed errors (in kcal/mol) change as follows: 4.3 (HF), −11.2 (OptX), −14.6 (OHLYP), −17.8 (OLYP), −18.3 (OreLYP). Thus, each successive change makes the magnitude of the error larger.

In order to see which functionals provide the smallest overall errors for all five properties of interest (IP, EA, IE, EE, and BDE), we show the average unsigned error (AUE) of all five properties (Tables 2, 3, 4, and the left side of 5) on the right side of Table 5. It is very interesting to compare B3LYP*, B3LYP, and CAM-B3LYP. They are very similar functionals, differing only in the percentage of HF exchange, which is given in Table 1. The results in the last column of Table 5 show that B3LYP is better than B3LYP*, and CAM-B3LYP is better than B3LYP. This tells us that, at least for the combination of B88X exchange and LYP correlation, more HF exchange is good for getting accurate results for the quantities important for CaO

dx.doi.org/10.1021/ct5000814 | J. Chem. Theory Comput. 2014, 10, 2291−2305

bond formation, and this is easily understood from the trends already discussed. Next, proceeding from B3LYP to CAM-B3LYP, the HF exchange at short-range is decreased by one percent and the HF exchange at long-range is increased by 45%. As a result, CAM-B3LYP is better than B3LYP by 2.2 kcal/mol for BDE, 0.7 kcal/mol for EA, 0.7 kcal/mol for EE, and 0.2 kcal/mol for the AUE. This result shows that increasing HF exchange only at long-range is helpful for this molecule. Similarly, we can compare the functionals PBE, HSE, and PBE0. They are also similar functionals, again differing only in HF exchange. HSE is 0.1 kcal/mol better for AUE than PBE0 and 5.2 kcal/mol better than PBE. Even though PBE0, which has 25% HF exchange at long-range (and short-range), is a little worse than HSE, which has zero HF exchange at long-range, the result still shows that more HF exchange is better. The reason why HF exchange is good for CaO is that EE is the dominant error among five components; more HF exchange increases the excitation energy of Ca^+, which decreases the error in EE because all the exchange-correlation functionals predict a smaller EE than the experimental value. However, fixing only the error in EE is not enough to design a good functional. HFLYP has the smallest error in EE but it has the second largest error in AUE. A good density functional should predict all five terms in eq 2 accurately, not just the one on the left-hand side.

The more components a functional can predict well, the less likely the accurate value of BDE comes from the cancellation of errors. A low AUE is obtained in Table 5 for functionals that predict all five properties relatively accurately. We can see from the average unsigned errors in Table 5 that M05 is the best functional for CaO. Then come B1LYP, M06-2X, PW6B95, M08-HX, B97-3, M06, and M05-2X. Several of the Minnesota functionals predict good results for CaO, but the performance of M11 is especially disappointing when one considers its high HF exchange percentage.

There are 53 methods in Table 5, and the 23 of these methods that have the smallest AUE (the first 23 functional in the last column of Table 5) are nonlocal, that is, have a nonzero amount of Hartree−Fock exchange. The best local functionals are MOHLYP (24th in the AUE ranking), revTPSS (27th), OreLYP (28th), BLYP (31th), M06-L (33rd), and M11-L (35th). In order to allow easier comparison of the individual errors in a given functional, we show errors in graphical form in Figure 2. From the figures, we can see clearly that hybrid functionals generally have smaller errors in each component, as compared to local functionals. For local functionals, the contribution of BDE and EE quantities to the AUE is larger than those of IE, IP, and EA quantities. For hybrid functionals, EE contributes more than other components.

5.2. Dipole Moment. In order to assess the accuracy of the density yielded by each functional, we calculated the dipole moment because for a diatomic molecule the dipole moment is an observable that tells how the charge is distributed between the two centers. If precisely one electron were transferred, we can calculate from the internuclear distance that the dipole moment of CaO would be 8.75 D. This is very close to the actual dipole moment of 8.73 D. Thus, although it is an idealization to think of CaO as being composed of Ca^+(d) and O^-, the actual fractional charge transfer is very close to 1.00 electron. A density functional that treats the bond properly should predict this accurately. The errors in the calculated dipole moments are given in Table 6, where the exchange−correlation functionals are ordered according to the unsigned error. Ideally, we would want a functional that ranks well both in the AUE ranking of Table 5 and the dipole ranking of Table 6. The functional with the best average ranking is B1LYP

Table 6. Signed Errors of the Dipole Moment (in debye) of CaO, Sorted in the Order of Increasing Unsigned Error[a]

name	dipole moment	SE
τ-HTCHhyb	8.79	0.06
B3LYP	8.80	0.07
TPSSh	8.64	−0.09
MN12-L	8.62	−0.11
B3LYP*	8.59	−0.14
M06-L	8.57	−0.16
B97-1	8.90	0.17
B1LYP	8.96	0.23
O3LYP	8.44	−0.29
HSE	9.03	0.30
M05	9.07	0.34
PBE0	9.08	0.35
PW6B95	9.08	0.35
M06	9.09	0.36
N12-SX	9.11	0.38
B97−3	9.13	0.40
M11-L	8.28	−0.45
MPW1B95	9.21	0.48
MN12-SX	9.23	0.50
revTPSSVP86	8.21	−0.52
revTPSS	8.21	−0.52
GVWN5	8.13	−0.60
MPWLYP1M	8.09	−0.64
BPW91	8.08	−0.65
PBEsol	8.08	−0.66
SOGGA11	8.07	−0.66
mPWPW	8.06	−0.67
SOGGA	8.05	−0.68
BP86	8.05	−0.68
PW91	8.03	−0.70
PBE	8.01	−0.72
N12	7.94	−0.79
OLYP	7.92	−0.81
CAM-B3LYP	9.55	0.82
OreLYP	7.90	−0.83
BLYP	7.90	−0.83
SOGGA11-X	9.66	0.93
MOHLYP	7.77	−0.96
MPWB1K	9.70	0.97
OHLYP	7.75	−0.98
ωB97X-D	9.71	0.98
M06-2X	9.82	1.09
M08-HX	9.82	1.09
M08-SO	9.83	1.10
OptX	7.56	−1.17
M05-2X	9.94	1.21
PBEX	7.45	−1.28
ωB97X	10.05	1.32
M11	10.09	1.36
ωB97	10.20	1.47
HFLYP	11.28	2.55
HF	11.30	2.57
B88X	12.93	4.20

[a]The CCSDT benchmark value of the dipole moment of CaO is 8.73 D.

(second for AUE and eighth for dipole, for an average ranking of 5. No other functional is ranked in the top nine in both the energetic and charge distribution categories; other functionals that do relatively well in this regard (with their average ranking in parentheses) are M05 (6), B3LYP (8.5), PW6B95 (8.5), B97-1 (9.0), HSE (10.0), and M06 (10.5).

Visual examination of Table 2 shows an anticorrelation of predicted BDE with predicted charge on Ca (this would also translate into an anticorrelation of predicted BDE with predicted dipole moment and, for the majority of functions, since most of them underestimate the bond energy, an anticorrelation of the dipole moment with accuracy of the bond energy). To quantify the anticorrelation we computed the Pearson correlation coefficient r of the 53 BDE values in Table 2 with the 53 values of the partial atomic charge on Ca. We obtained $r = -0.783$; the sign being negative corresponds to larger BDEs being associated with smaller dipole moments, which is counterintuitive, but the value of $|r|$ being closer to unity than zero shows that there is indeed an anticorrelation. Therefore, the accuracy of the predicted bond energy is related to the predicted amount of charge transfer, and we next seek to uncover the factors controlling the charge distribution.

A calculated dipole moment that is too large means that there is too much charge transferred. For some functionals, we found that a prediction of a small ionization potential for Ca and a large electron affinity of O are associated with a prediction of too large a dipole moment, which is easy to understand. However, we also have some functionals that predict a large IP and small EA but nevertheless yield too large of a dipole moment. So, the dipole moments are not rationalized by considering the IP and EA. However, the dipole moments can be rationalized by the charge distributions of the key orbitals.

5.3. Potential Curves and Orbital Analysis. The CaO molecule has a low-lying triplet state as well as the singlet state we have been discussing so far, and it will be informative to consider the potential curves of both the singlet and the triplet state. These two curves are given for two of the functionals in Figure 3. The reason we illustrate the trends with these two functionals is that M05 has the smallest AUE and MPWB1K has an AUE that is larger by 2.9 kcal/mol, and their predicted dipole moments differ by 0.63 debye. Figure 3 shows that the two functionals give similar potential curves. Figure 4 compares our potential curves calculated by M05 and MPWB1K with experimental results.[16] Only CaO singlet is presented in Figure 4. The predicted R_e by M05 and MPWB1K is a little smaller than the experimental value. M05 and MPWB1K agree well with the experimental curve before R_e. M05 predicts the energy higher than the experimental energy after R_e, and MPWB1K predicts the energy lower than the experimental energy after 2.2 Å. Besides, there is a change of slope (at 2.078 Å) on the MPW1K curve. Since we employ the stable=opt keyword of *Gaussian 09*, before this point the energy was calculated by restricted DFT, and after this point the energy was calculated by unrestricted DFT.

Table 7 shows the orbital occupancies in the two states at large internuclear distance $R = 10$ Å, at the equilibrium internuclear distance $R = R_e$, and at the intermediate distance of $R = 4$ Å. Notice that the orbitals are labeled by their energetic ordering and their dominant symmetry. Consider the $3\pi_x$, $3\pi_y$, and 8σ orbitals at the equilibrium geometry. If the 8σ orbital were localized on Ca the partial atomic charges would be about zero (six valence electrons would be on O and 2 on Ca). Thus,

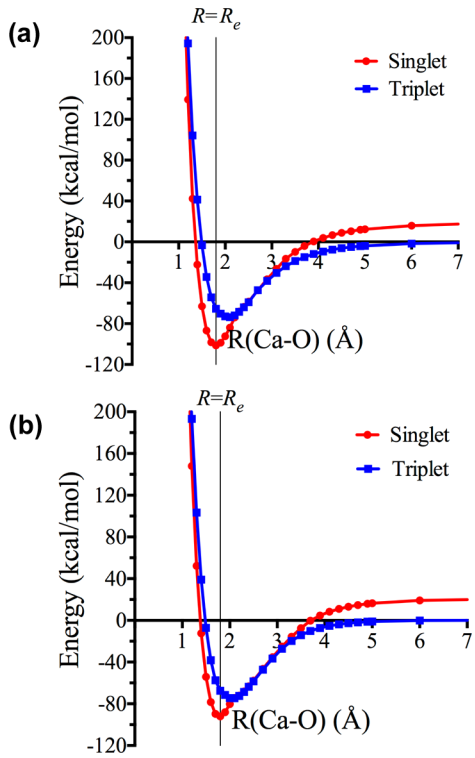

Figure 3. Potential curves of singlet CaO and triplet CaO, (a) calculated with the M05 exchange-correlation functional and (b) calculated with the MPWB1K exchange−correlation functional. The thin vertical line shows $R = R_e$.

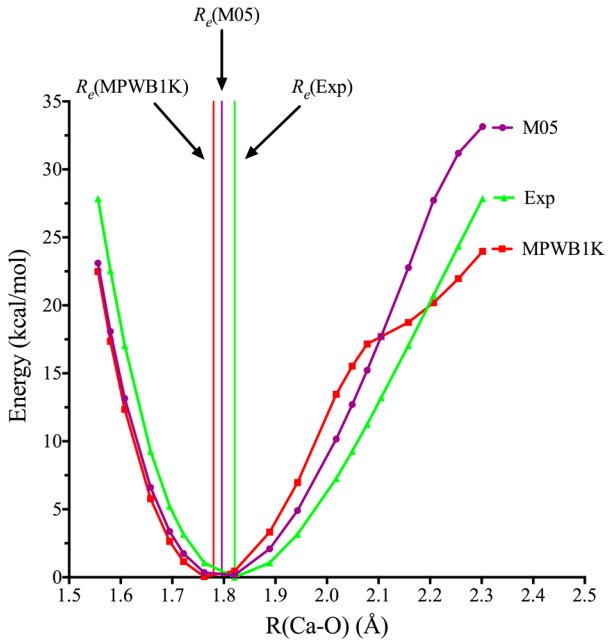

Figure 4. Potential curves of CaO singlet, calculated with M05 and MPWB1K exchange−correlation functionals and compared to the experimental RKR curve. R_e (MPWB1K) = 1.780 Å, R_e (M05) = 1.796 Å, R_e (expt.) = 1.821 Å.

it is the extent of delocalization of the orbital that determines the ionic character.

We used NBO analysis to ascertain the partial atomic charge contribution of each molecular orbital. (Even though the charges given by NBO analysis are different from the charges

dx.doi.org/10.1021/ct5000814 | J. Chem. Theory Comput. 2014, 10, 2291−2305

Table 7. Occupation of Selected Singlet and Triplet CaO Orbitals at Selected Internuclear Distances

M05 or MPWB1K	7σ (O2s)	8σ (OpσCa 3dσ)	$3\pi_x$ (Opπ)	$3\pi_y$ (Opπ)	9σ (Ca4s)
Ca + O (singlet, R_e)	2	2	2	2	0
Ca + O (triplet, R_e)	2	1	2	2	1
M05		7σ (O2s)	8σ (Opσ)	$3\pi_x$ (Opπ)	$3\pi_y$ (Opπ)	9σ (Ca4s)
Ca + O (singlet, 4−10 Å)		2	2	0	2	2
Ca + O (triplet, 4−10 Å)		2	1	1	2	2
MPWB1K	7σ (O2s)	8σ (OpσCa 3dσ)	$3\pi_x$ (Opπ)	$3\pi_y$ (Opπ)	9σ (OpσCa4s)
Ca + O (singlet, 4 Å)	2	2	2	2	0
MPWB1K		7σ (O2s)	8σ (Ca4s)	$3\pi_x$ (Opπ)	$3\pi_y$ (Opπ)	9σ (Opσ)
Ca + O (singlet, 10 Å)		2	2	2	2	0
Ca + O (triplet, 4−10 Å)		2	2	1	2	1

we calculated from the dipole moment, and we do not recommend NBO analysis for calculating partial atomic charges for molecular modeling, NBO analysis does provide useful information about how much charge transfer comes from individual molecular orbitals.) NBO analysis of the M05 charge distribution yields Ca having a partial atomic charge q of +1.34, and O having q = −1.34; these 1.34 units of charge consist of 0.70 units from the two 3π orbitals and 0.64 charges from the 8σ orbital. For MPWB1K, Ca has q = +1.39, and O has q = −1.39; for this functional the charge transfer consists of 0.74 units from the two 3π orbitals and 0.65 units from the 8σ orbital. This analysis shows that the two density functionals exhibit qualitatively similar trends in how the charge is transferred, but there is a bigger difference in the π manifold than in the σ manifold. The various density functionals predict different characters for these three orbitals, and we find that these predictions are correlated to the predicted dipole moment.

In order to see the correlation between dipole moment and bond energy, we choose six functionals, B3LYP, BLYP, MOHLYP, MPWB1K, M05, and M06-2X, and we compare some of the properties calculated by these functionals in Table 8, where the functionals are listed in order of increasing dipole moment. As we can see, of the six functionals compared, B3LYP has the smallest error for the dipole moment, but MPWB1K has the smallest error for BDE. The largest error comes from the excitation energy for all six of these functionals, and the most interesting feature in Table 8 is the good correlation between the excitation energy and the dipole moment but not with the IP or the EA.

The second and third rows in Table 8 show the charge distributions in the 8σ, $3\pi_x$, and $3\pi_y$ orbitals, as obtained from NBO analysis. Comparing the numbers in these rows to those in the first row shows, as expected, that a smaller percentage of electrons on Ca is associated with a larger dipole moment.

For the $3\pi_x$ and the $3\pi_y$ orbital of CaO, B3LYP has a charge distribution with 8.6% on Ca (mainly in a d orbital) and 91% on O in a p orbital, whereas BLYP has the distribution at 9.3% and 91%.; similarly, for the 8σ bonding orbital of CaO, B3LYP gives the charge distribution as 16% on Ca (mainly d) and 84% on O, whereas BLYP gives the charge distribution as 18% on Ca (mainly d) and 82% on O (p). Therefore, it is mainly a Ca d orbital that is dominating these two-center orbitals and is forming the bond with oxygen, and these distributions are consistent with B3LYP predicting a greater dipole moment (more electrons on O and less electrons on Ca) than BLYP, as seen previously in Table 6.

Proceeding from left to right in Table 8 shows that as the calculated cation excitation energy increases, making the 3d orbital on Ca less attractive, it becomes harder to delocalize charge from the O2p orbital to the Ca3d orbital in the 8σ, $3\pi_x$, and $3\pi_y$ bonding orbitals; this increases the dipole moment but it decreases the covalency, and the decreased delocalization in the bonding orbital decreases the bond energy. This illustrates in terms of orbitals how the EE effects bond dissociation energy.

When R(Ca−O) is larger than 2.3 Å, the ground state of CaO is best described as Ca singlet combined with O triplet because triplet O is lower in energy than singlet O when it is separated from Ca by this distance. To correctly describe the O atom in a triplet state, spin-polarized KS-DFT or the unrestricted HF method needs to be used.

Figures 5 and 6 show the relevant orbital energies for the singlet and the triplet for the M05 and MPWB1K density functionals. As seen in the figures, the derivatives of the orbital energy curves for the singlet are are discontinuous where the restricted KS-DFT solution becomes unstable. At R larger than the instability point, the variationally lowest-energy solution is spin-polarized, whereas at smaller R the spin-restricted solution is stable. We find that the restricted solution is stable at the equilibrium geometry for all functionals, and all functionals yield nonsmooth orbital energy curves because of the instability of the restricted solution at large R.

For the M05 functional, when R(Ca−O) is smaller than 2.3 Å but in the vicinity of $R = R_e$, singlet CaO is well described as a

Table 8. Comparison of Chemical Properties of CaO Calculated by Six Functionals

property	MOHLYP	BLYP	B3LYP	M05	MPWB1K	M06-2X	expt.[a]
dipole moment (debye)	7.8	7.9	8.8	9.1	9.7	9.8	8.7
charge distribution of 8σ orbital	18.2% Ca	18.0% Ca	16.0% Ca	15.7% Ca	14.0% Ca	14.1% Ca	
	81.8% O	82.0% O	84.0% O	84.3% O	86.0% O	85.9% O	
charge distribution of $3\pi_x$ and $3\pi_y$ orbitals	9.3% Ca	9.3% Ca	8.6% Ca	8.5% Ca	8.3% Ca	8.0% Ca	
	90.7% O	90.7% O	91.4% O	91.5% O	91.7% O	92.0% O	
BDE (kcal/mol)	111.8	118.6	104.5	101.0	91.6	89.4	96.1
IP (kcal/mol)	136.9	139.6	141.6	141.7	136.1	144.2	141.0
EA (kcal/mol)	35.4	42.1	38.8	31.6	26.3	32.5	33.9
EE (kcal/mol)	24.5	25.9	27.5	27.4	29.4	32.7	39.1
IE (kcal/mol)	237.8	242.0	234.9	238.5	230.8	233.9	242.3

[a]Experimental values are from references 39, 40, 42−44.

dx.doi.org/10.1021/ct5000814 | J. Chem. Theory Comput. 2014, 10, 2291−2305

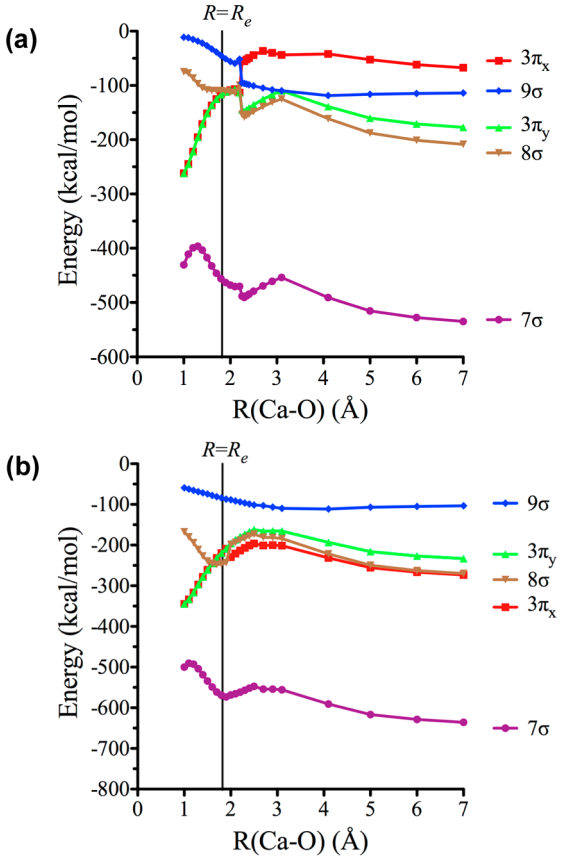

Figure 5. Orbital energies of the CaO singlet state, as calculated with the M05 exchange-correlation functional. The thin vertical line shows $R = R_e$. The molecule is on the z axis. The 7σ, 8σ, and $3\pi_y$ orbitals are doubly occupied both at R_e (1.821 Å) and at 7 Å. At R_e, the 8σ is doubly occupied, and 9σ is empty. At 7 Å, 9σ is doubly occupied, and $3\pi_x$ is empty. (b) Orbital energies of the CaO triplet state, as calculated with the M05 exchange-correlation functional. The thin vertical line shows $R = R_e$. The molecule is on the z axis. At R_e (1.821 Å), the 7σ, $3\pi_x$, and $3\pi_y$ orbitals are doubly occupied, and the 8σ and 9σ orbitals are singly occupied. At 7 Å, the 7σ, 8σ, and $3\pi_y$ orbitals are doubly occupied, and the 8σ and $3\pi_x$ orbitals are singly occupied.

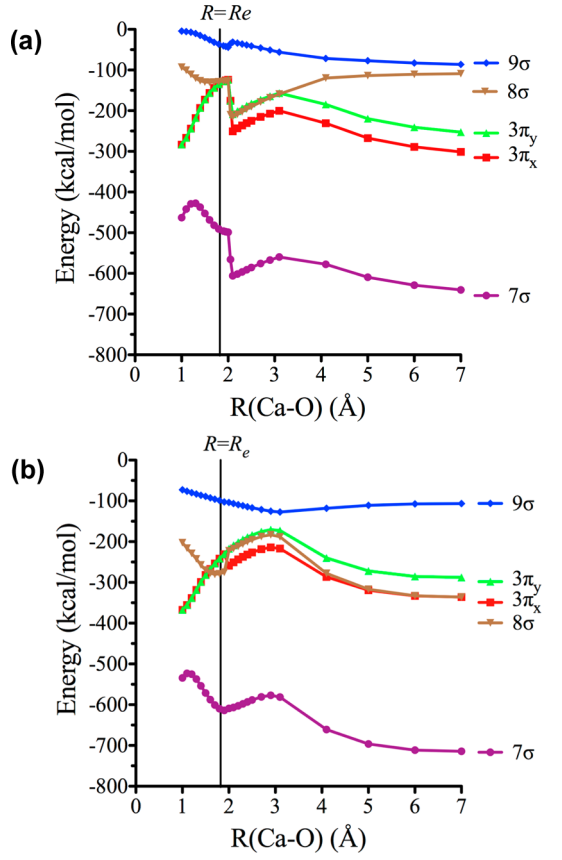

Figure 6. Orbital energies of CaO singlet state, as calculated with the MPWB1K exchange−correlation functional. The thin vertical line shows $R = R_e$. The molecule is on the z axis. The 7σ, 8σ, $3\pi_x$, and $3\pi_y$ orbitals are doubly occupied both at R_e (1.821 Å) and at 7 Å. (b) Orbital energies of the CaO triplet state, as calculated with the MPWB1K exchange−correlation functional. The thin vertical line shows $R = R_e$. The molecule is on the z axis. At R_e (1.821 Å), 7σ, $3\pi_x$, and $3\pi_y$ orbitals are doubly occupied; 8σ and 9σ orbitals are singly occupied. At 7 Å, the 7σ, 8σ, and $3\pi_y$ orbitals are doubly occupied, and the 9σ and $3\pi_x$ orbitals are singly occupied.

combination of Ca^+ doublet and O^- doublet with the partial atomic charge on Ca in the range 0.9 to 1.1. When R(Ca−O) becomes smaller than R_e, Figure 7 shows that the charge on Ca decreases significantly, and CaO is best described as nonionic Ca singlet and O singlet.

Figure 8 shows the orbitals of 8σ, 3π, and 9σ orbitals of CaO at R_e as calculated by M05. According to the first section Table 7, the difference between the singlet and triplet states of CaO at R_e with the M05 functional is that the singlet has two electrons in the 8σ orbital and no electrons in 9σ, and the triplet has one electron in the 8σ orbital and one in the 9σ orbital. The second section of Table 7 shows that the difference between the singlet and triplet states of CaO at 10 Å is that the singlet has two electrons in the 8σ orbital, no electrons in $3\pi_x$, and two electrons in 9σ, whereas the triplet has one electron in the 8σ orbital, one electron in the $3\pi_x$ orbital, and two electrons in the 9σ orbital.

For MPWB1K, the orbital occupancies at R_e are the same as for M05; thus, the singlet has two electrons in the 8σ orbital and no electrons in the 9σ orbital, but the triplet has one electron in the 8σ orbital and one in the 9σ orbital. However, the difference between singlet and triplet state of CaO at 10 Å is that the singlet has two electrons in the 8σ orbital, two electrons in the $3\pi_x$ orbital, and zero electrons in the 9σ orbital, and the triplet has two electrons in the 8σ orbital, one electron in the $3\pi_x$ orbital, and one electron in the 9σ orbital.

At the equilibrium distance, both functionals have the 8σ orbital as the HOMO orbital and the 9σ orbital as the LUMO orbital for singlet CaO. However, as a result of the occupancies explained in the previous two paragraphs, for M05, when we start at R_e and increase the bond distance, the singlet state has two electrons that transfer from the $3\pi_x$ orbital to the 9σ orbital, whereas the triplet state has one electron that transfers from the $3\pi_x$ orbital to the 9σ orbital. In contrast, for MPWB1K, when we start at R_e and increase the bond distance, the singlet state has no electron transferred, whereas the triplet state has one electron that transfers from the $3\pi_x$ orbital to the 8σ orbital. Table 7 also illustrates that Ca is using a $3d\pi_x$ orbital instead of the 4s orbital to form the bond with oxygen since the 8σ orbital (not the 9σ orbital) is occupied by two electrons at R_e.

Figure 5 shows the singlet orbital energies calculated by the M05 functional, and Figure 6 shows the same quantities as calculated by the MPWB1K functional; the difference between these figures is the order of these orbitals at large distances. For

dx.doi.org/10.1021/ct5000814 | J. Chem. Theory Comput. 2014, 10, 2291−2305

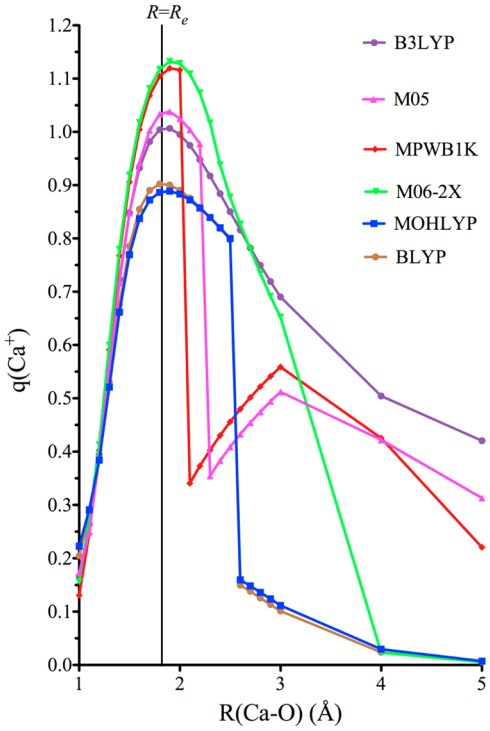

Figure 7. Charge of Ca versus R(Ca−O). The charge of Ca at each distance is calculated by dividing dipole moment by the distance at that point. Six exchange-correlation functionals were employed in this figure.

M05, when R is larger than 2.3 Å, orbital $3\pi_x$ is higher in energy and 9σ is lower in energy. For MPWB1K at large distance, 9σ is higher in energy, and $3\pi_x$ is lower in energy. In comparison to the singlet case, Figures 5b and 6b show that the two functionals do give similar orbital energies for the triplet state. The chief difference between these two figures is the energy gap between 8σ and 9σ orbitals at large distance. MPWB1K predicts a larger energy gap between the 8σ and 9σ orbitals of CaO triplet at large distance. For both the triplet and the singlet, the $3\pi_x$ and $3\pi_y$ orbitals are degenerate only at small bond distance, but they have an energy gap of about 50 kcal/mol at 10 Å—except for the M05 singlet, which has an energy gap between the $3\pi_x$ and $3\pi_y$ orbitals of about 100 kcal/mol.

6. CONCLUSIONS

CaO is a multireference system according to the T_1, TAE(T), B_1, and M diagnostics. We found that the predicted BDE is anticorrelated with the predicted dipole moment, with a larger dipole moment leading to a smaller BDE. At the equilibrium distance CaO is made up of $Ca^+(d)$ and O^-. The partial charges we calculated from the experimental dipole moment are $Ca^{+0.998}$ and $O^{-0.998}$. By comparing dipole moments and orbital makeups predicted by different density functionals, we found that the valence-orbital charge distributions between the two centers can be used to explain the trends in the predicted dipole moment. Even if we have a good dipole moment (i.e., a good first moment of the density), we cannot guarantee good results for all the contributions to the bond energy of CaO. The error of the BDE of CaO was partitioned into errors from four sources: the ionization potential (IP), the electron affinity (EA), the atomic excitation energy (EE) of the metal cation to prepare the valence state, and the interaction energy between prepared states (IE). The more components a functional can

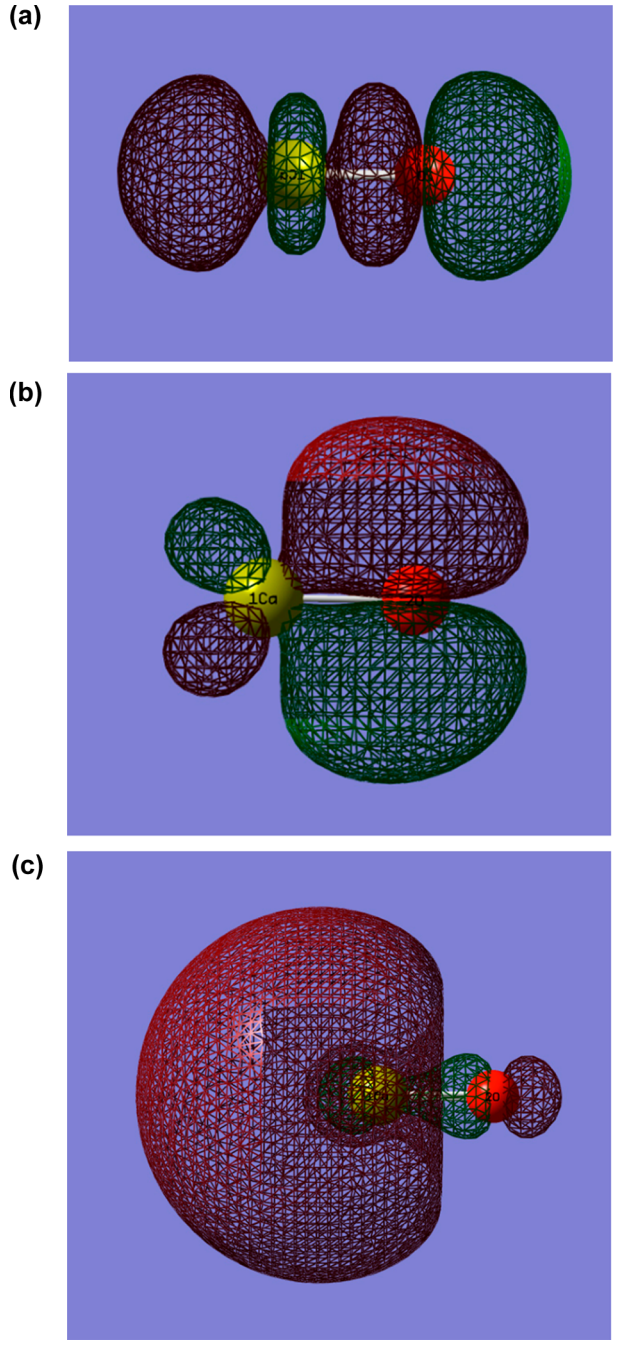

Figure 8. (a) 8σ orbital, (b) 3π orbital, and (c) 9σ orbital of CaO at $R = R_e$, calculated by M05. Ca is on the left, and O is on the right.

predict accurately, the less likely that accurate results come from fortuitous cancellation of error. Typically the excitation energy and the interaction energy contribute more to the errors than other components, with the error in the excitation energy of Ca^+ being the largest factor.

The excitation energy error is dominated to a large extent by near-degeneracy angular correlation of the s and d orbitals of Ca^+; a lower excitation energy leads to less delocalization of the σ bonding orbital (and hence a smaller dipole moment) and a higher bond energy. This is further confirmed by Table 9, which shows that the usual trend is that lower excitation energy (EE) leads to higher bond dissociation energy (BDE), anticorrelated with higher partial atomic charge on Ca. To

dx.doi.org/10.1021/ct5000814 | J. Chem. Theory Comput. 2014, 10, 2291−2305

Table 9. Bond Dissociation Energy, Charge on Ca in CaO, and Excitation Energy of $Ca^+(s)$[a]

	BDE[b]	q (Ca)	EE $Ca^+(s)$
MN12-L	96.2	0.99	10.5
ωB97	102.5	1.17	16.3
M06-L	114.4	0.98	16.4
MN12-SX	98.0	1.06	17.2
τ-HTCHhyb	113.4	1.01	18.8
M11-L	91.9	0.95	19.3
N12-SX	109.5	1.04	20.5
OreLYP	116.8	0.90	20.8
M11	110.4	1.15	21.0
OLYP	118.9	0.91	21.3
revTPSS	115.3	0.94	21.5
BPW91	123.5	0.92	21.9
TPSSh	110.5	0.99	21.9
revTPSSVP86	116.8	0.94	22.5
mPWPW	124.9	0.92	22.8
N12	117.3	0.91	22.8
O3LYP	110.8	0.96	22.8
BP86	124.6	0.92	23.1
PW91	126.3	0.92	23.7
ωB97X-D	103.3	1.11	23.8
B97-1	106.4	1.02	23.9
PBEsol	132.8	0.92	24.1
PBE	124.3	0.92	24.3
MOHLYP	111.8	0.89	24.5
OHLYP	101.4	0.89	24.5
SOGGA	132.4	0.92	24.6
M06	102.0	1.04	25.0
B97-3	100.8	1.04	25.4
SOGGA11-X	92.6	1.10	25.7
BLYP	118.6	0.90	25.9
GVWN5	146.2	0.93	26.3
PBE0	103.0	1.04	26.4
HSE	102.8	1.03	26.7
M05-2X	93.6	1.14	26.9
M08-HX	94.7	1.12	27.1
B3LYP*	110.0	0.98	27.2
MPWLYP1M	115.4	0.92	27.3
M05	101.0	1.04	27.4
B3LYP	104.5	1.01	27.5
PW6B95	102.8	1.04	27.7
OptX	83.4	0.86	27.9
SOGGA11	123.0	0.92	28.1
CAM-B3LYP	102.3	1.09	28.2
MPW1B95	101.5	1.05	28.2
B1LYP	97.2	1.02	28.7
ωB97X	101.4	1.15	28.8
MPWB1K	91.6	1.11	29.4
M08-SO	90.1	1.12	31.4
B88X	−13.0	1.48	32.2
M06-2X	89.4	1.12	32.7
PBEX	85.3	0.85	34.6
HFLYP	48.3	1.29	35.7
HF	12.0	1.29	43.4

[a]Sorted in order of increasing magnitude of excitation energy. [b]The experiment value of BDE is 96.1 kcal/mol.[39,40]

get an accurate bond energy for the right reason, one must balance the localization and delocalization tendencies.

Combining what we learned from the orbital analyses with the data in Table 8, we infer that the important factors controlling the calculated bond energy and calculated dipole moment are the extent of delocalization, the amount of charge transfer, and the covalent bonding in the 8σ, $3\pi_x$, and $3\pi_y$ orbitals. If functional A predicts that the 8σ, $3\pi_x$, and $3\pi_y$ orbitals are more delocalized than the ones predicted by functional B, then the dipole moment predicted by functional A is smaller than the dipole moment predicted by functional B. However, the increased delocalization increases the calculated bond energy. From the NBO analysis, we found that MPWB1K predicts the 8σ orbital, the $3\pi_x$ orbital, and the $3\pi_y$ orbital to be more delocalized than the ones predicted by M05. Therefore, MPWB1K predicts a larger dipole moment than M05 but a smaller bond energy.

The present analysis suggests that a good approach toward making exchange−correlation functionals more accurate is try to design functionals that predict well all five of the properties studied here and especially to place more emphasis than previous work on atomic excitation energies. We found here that one way to get a more accurate atomic excitation energy is to increase the amount of HF exchange for each functional, but it is well-known that there is a trade-off in this kind of parametrization because high Hartree−Fock exchange often brings in static correlation error for many systems; therefore, a broader strategy is warranted. It will be interesting to carry out this kind of analysis for more molecules to further guide future density functional design.

AUTHOR INFORMATION

Corresponding Author

*Email: truhlar@umn.edu.

Notes

The authors declare no competing financial interest.

ACKNOWLEDGMENTS

This work was supported in part by the Air Force Office of Scientific Research by Grant No. FA9550-11-1-0078.

REFERENCES

(1) Mok, D. K. W.; Neumann, R.; Handy, N. C. *J. Phys. Chem.* **1996**, *100*, 6225−6230.
(2) Handy, N. C.; Cohen, A. J. *Mol. Phys.* **2001**, *99*, 403−412.
(3) Hollett, J. W.; Gill, P. M. W *J. Chem. Phys.* **2011**, *134*, 114111.
(4) Buijse, M. A.; Baerends, E. J. *J. Chem. Phys.* **1990**, *93*, 4129−4141.
(5) Handy, N. C. *Mol. Phys.* **2009**, *107*, 721−726.
(6) Cohen, A. J.; Handy, N. C. *Mol. Phys.* **2001**, *99*, 607−615.
(7) Jackels, C. F.; Shavitt, I. *Theor. Chim. Acta* **1981**, *58*, 81−96.
(8) Shavitt, I. In *Advanced Theories and Computational Approaches to the Electronic Structure of Molecules*; Dykstra, C. E., Ed.; D. Reidel: Dordrecht, 1984; pp 185−196.
(9) Truhlar, D. G. *J. Comput. Chem.* **2007**, *28*, 73−86.
(10) Kohn, W.; Becke, A. D.; Parr, R. G. *J. Phys. Chem.* **1996**, *100*, 12974−12980.
(11) Peverati, R.; Truhlar, D. G. *Philos. Trans. R. Soc. A* **2014**, *372*, 1−51.
(12) Sullivan, M. B.; Iron, M. A.; Redfern, P. C.; Martin, J. M. L.; Curtiss, L. A.; Radom, L. *J. Phys. Chem. A* **2003**, *107*, 5617−5630.
(13) Haworth, N. L.; Sullivan, M. B.; Wilson, A. K.; Martin, J. M. L.; Radom, L. *J. Phys. Chem. A* **2005**, *109*, 9156−9168.
(14) England, W. B. *Chem. Phys.* **1980**, *53*, 1−21.
(15) Khalil, H.; Brites, V.; Quéré, F. Le.; Léonard, C. *Chem. Phys.* **2011**, *386*, 50−55.
(16) Murthy, N. S.; Prahllad, U. D.; Rao, T. V. R.; Naidu, G. T. *Indian J. Pure Appl. Phys.* **1980**, *18*, 818−821.

(17) Yoshimine, M. *J. Phys. Soc. Jpn.* **1968**, *25*, 1100−1119.
(18) Woon, D. E.; Dunning, T.; K, J. *J. Chem. Phys.* **1995**, *103*, 4572−4585.
(19) Koput, J.; Peterson, K. A. *J. Phys. Chem. A* **2002**, *106*, 9595−9599.
(20) Douglas, M.; Kroll, N. M. *Ann. Phys.* **1974**, *82*, 89−155.
(21) Hess, B. A. *Phys. Rev. A* **1985**, *32*, 756−763.
(22) Hess, B. A. *Phys. Rev. A* **1986**, *33*, 3742−3748.
(23) Jansen, G.; Hess, B. A. *Phys. Rev. A* **1989**, *39*, 6016−6017.
(24) Vasiliu, M.; Feller, D.; Gole, J. L.; Dixon, D. A. *J. Phys. Chem. A* **2010**, *114*, 9349−9358.
(25) Frisch, M. J.; Trucks, G. W.; Schlegel, H. B.; Scuseria, G. E.; Robb, M. A.; Cheeseman, J. R.; Scalmani, G.; Barone, V.; Mennucci, B.; Petersson, G. A.; Nakatsuji, H.; Caricato, M.; Li, X.; Hratchian, H. P.; Izmaylov, A. F.; Bloino, J.; Zheng, G.; Sonnenberg, J. L.; Hada, M.; Ehara, M.; Toyota, K.; Fukuda, R.; Hasegawa, J.; Ishida, M.; Nakajima, T.; Honda, Y.; Kitao, O.; Nakai, H.; Vreven, T.; Montgomery, J. A., Jr.; Peralta, J. E.; Ogliaro, F.; Bearpark, M.; Heyd, J. J.; Brothers, E.; Kudin, K. N.; Staroverov, V. N.; Kobayashi, R.; Normand, J.; Raghavachari, K.; Rendell, A.; Burant, J. C.; Iyengar, S. S.; Tomasi, J.; Cossi, M.; Rega, N.; Millam, N. J.; Klene, M.; Knox, J. E.; Cross, J. B.; Bakken, V.; Adamo, C.; Jaramillo, J.; Gomperts, R.; Stratmann, R. E.; Yazyev, O.; Austin, A. J.; Cammi, R.; Pomelli, C.; Ochterski, J. W.; Martin, R. L.; Morokuma, K.; Zakrzewski, V. G.; Voth, G. A.; Salvador, P.; Dannenberg, J. J.; Dapprich, S.; Daniels, A. D.; Farkas, Ö.; Foresman, J. B.; Ortiz, J. V.; Cioslowski, J.; Fox, D. J. *Gaussian 09*, revision C01; Gaussian, Inc., Wallingford CT, 2009.
(26) Lee, T. J.; Taylor, P. R. *Int. J. Quantum Chem. Symp.* **1989**, *23*, 199−207.
(27) Karton, A.; Rabinovich, E.; Martin, J. M. L.; Ruscic, B. *J. Chem. Phys.* **2006**, *125*, 144108.
(28) Schultz, N. E.; Zhao, Y.; Truhlar, D. G. *J. Phys. Chem. A* **2005**, *109*, 11127−11143.
(29) Tishchenko, O.; Zheng, J.; Truhlar, D. G. *J. Chem. Theory. Comput.* **2008**, *4*, 1208−1219.
(30) Zhao, Y.; Tishchenko, O.; Gour, J. R.; Li, W.; Lutz, J. J.; Piecuch, P.; Truhlar, D. G. *J. Phys. Chem. A* **2009**, *113*, 5786−5799.
(31) Werner, H.-J.; Knowles, P. J.; Manby, F. R.; Schütz, M.; Celani, P.; Knizia, G.; Korona, T.; Lindh, R.; Mitrushenkov, A.; Rauhut, G.; Adler, T. B.; Amos, R. D.; Bernhardsson, A.; Berning, A.; Cooper, D. L.; Deegan, M. J. O.; Dobbyn, A. J.; Eckert, F.; Goll, E.; Hampel, C.; Hesselmann, A.; Hetzer, G.; Hrenar, T.; Jansen, G.; Köppl, C.; Liu, Y.; Lloyd, A. W.; Mata, R. A.; May, A. J.; McNicholas, S. J.; Meyer, W.; Mura, M. E.; Nicklaß,A.; Palmieri, P.; Pflüger, K.; Pitzer, R. M.; Reiher, M.; Shiozaki, T.; Stoll, H.; Stone, A. J.; Tarroni, R.; Thorsteinsson, T.; Wang, M.; and Wolf, A. *Molpro*, version 2010.1; University of Birmingham: Birmingham, 2010.
(32) Roos, B. O.; Taylor, P. R.; Siegbahn, P. E. M. *Chem. Phys.* **1980**, *48*, 157−173.
(33) Helgaker, T.; Jorgensen, P.; Olsen, J. *Modern Electronic Structure Theory*; Wiley: Chichester, 2000; p 188.
(34) Valiev, M.; Bylaska, E. J.; Govind, N.; Kowalski, K.; Straatsma, T. P.; van Dam, H. J. J.; Wang, D.; Nieplocha, J.; Apra, E.; Windus, T. L.; de Jong, W. A. *Comput. Phys. Commun.* **2010**, *181*, 1477−1489.
(35) Becke, A. D. *Phys. Rev. A* **1988**, *38*, 3098−3100.
(36) Lee, C.; Yang, W.; Parr, R. G. *Phys. Rev. B* **1988**, *37*, 785−789.
(37) Adamo, C.; Barone, V. *Chem. Phys. Lett.* **1997**, *274*, 242−250.
(38) Zhao, Y.; Peverati, R.; Yang, K.; Truhlar, D. G. *MN-GFM 6.4*. See http://comp.chem.umn.edu/mn-gfm/ for details. (accessed June 8, 2013).
(39) Pedley, J. B.; Marshall, E. M. *J. Phys. Chem. Ref. Data.* **1983**, *12*, 967−1031.
(40) Lide, D. R. In *Handbook of Chemistry and Physics*, 87th ed.; Lide, D. R., Ed.; CRC Press: Boca Raton, 2006; p 9−89.
(41) Foster, J. P.; Weinhold, F. *J. Am. Chem. Soc.* **1980**, *102*, 7211−7218.
(42) *Basic Atomic Data*; National Institute of Standards and Technology; http://physics.nist.gov/PhysRefData/Handbook/Tables/calciumtable1.htm (accessed June 8, 2013).
(43) *Chemguide*; http://www.chemguide.co.uk/atoms/properties/eas.html (accessed June 8, 2013).
(44) Moore, C. E. *Atomic Energy Levels*; U.S. Government Printing Office: Washington, DC, 1971; Vol. *I*, p 243.
(45) Stephens, P. J.; Devlin, F. J.; Chabalowski, C. F.; Frisch, M. J. *J. Phys. Chem.* **1994**, *98*, 11623−11627.
(46) Reiher, M.; Salomon, O.; Hess, B. A. *Theor. Chem. Acc.* **2001**, *107*, 48−55.
(47) Hamprecht, F. A.; Cohen, A. J.; Tozer, D. J.; Handy, N. C. *J. Chem. Phys.* **1988**, *109*, 6264−6271.
(48) Keal, T. W.; Tozer, D. J. *J. Chem. Phys.* **2005**, *123*, 121103.
(49) Perdew, J. P. *Phys. Rev. B* **1986**, *33*, 8822−8824.
(50) Perdew, J. P. In *Electronic Structure of Solids '91*; Ziesche, P., Eschrig, H., Eds.; Akademie Verlag: Berlin, 1991; pp 11−20.
(51) Yanai, T.; Tew, D.; Handy, N. *Chem. Phys. Lett.* **2004**, *393*, 51−57.
(52) Kohn, W.; Sham, L. J. *Phys. Rev.* **1965**, *140*, A1133−A1138.
(53) (a) Gáspár, R. *Acta Phys. Hung.* **1954**, *3*, 263−286. (b) Gáspár, R. *Acta Phys. Hung.* **1974**, *35*, 213−218.
(54) Vosko, S. H.; Wilk, L.; Nusair, M. *Can. J. Phys.* **1980**, *58*, 1200−1211.
(55) Roothaan, C. C. J. *Rev. Mod. Phys.* **1951**, *23*, 69−89.
(56) Pople, J. A.; Nesbet, K. R. *J. Chem. Phys.* **1954**, *22*, 571−572.
(57) McWeeny, R.; Dierksen, G. *J. Chem. Phys.* **1968**, *49*, 4852−4856.
(58) Valentin, C. D.; Pacchioni, G.; Bredow, T.; Dominguez-Ariza, D.; Illas, F. *J. Chem. Phys.* **2002**, *117*, 2299−2306.
(59) Heyd, J.; Scuseria, G. E.; Ernzerhof, M. *J. Chem. Phys.* **2003**, *118*, 8207−8215.
(60) Henderson, T. M.; Izmaylov, A. F.; Scalmani, G.; Scuseria, G. E. *J. Chem. Phys.* **2009**, *131*, 044108.
(61) Zhao, Y.; Schultz, N. E.; Truhlar, D. G. *J. Chem. Phys.* **2005**, *123*, 161103.
(62) Zhao, Y.; Schultz, N. E.; Truhlar, D. G. *J. Chem. Theory Comput.* **2006**, *2*, 364−382.
(63) Zhao, Y.; Truhlar, D. G. *Theor. Chem. Acc.* **2008**, *120*, 215−241.
(64) Zhao, Y.; Truhlar, D. G. *J. Chem. Phys.* **2006**, *125*, 194101.
(65) Zhao, Y.; Truhlar, D. G. *J. Chem. Theory Comput.* **2008**, *4*, 1849−1868.
(66) Peverati, R.; Truhlar, D. G. *J. Phys. Chem. Lett.* **2011**, *2*, 2810−2817.
(67) Peverati, R.; Truhlar, D. G. *J. Phys. Chem. Lett.* **2011**, *3*, 117−124.
(68) Peverati, R.; Truhlar, D. G. *Phys. Chem. Chem. Phys.* **2012**, *14*, 13171−13174.
(69) Peverati, R.; Truhlar, D. G. *Phys. Chem. Chem. Phys.* **2012**, *14*, 16187−16191.
(70) Schultz, N. E.; Zhao, Y.; Truhlar, D. G. *J. Phys. Chem. A* **2005**, *109*, 11127−11143.
(71) Zhao, Y.; Truhlar, D. G. *J. Phys. Chem. A* **2004**, *108*, 6908−6918.
(72) Adamo, C.; Barone, V. *J. Chem. Phys.* **1998**, *108*, 664−675.
(73) Peverati, R.; Truhlar, D. G. *J. Chem. Theory Comput.* **2012**, *8*, 2310−2319.
(74) Hoe, W.-M.; Cohen, A. J.; Handy, N. C. *Chem. Phys. Lett.* **2001**, *341*, 319−328.
(75) Thakkar, A. J.; McCarthy, S. P. *J. Chem. Phys.* **2009**, *131*, 134109.
(76) Perdew, J. P.; Burke, K.; Ernzerhof, M. *Phys. Rev. Lett.* **1996**, *77*, 3865−3868.
(77) Adamo, C.; Barone, V. *J. Chem. Phys.* **1999**, *110*, 6158−6170.
(78) Perdew, J.; Ruzsinszky, A.; Csonka, G. I.; Vydrov, O. A.; Scuseria, G. E. *Phys. Rev. Lett.* **2008**, *100*, 136406−136409.
(79) Perdew, J. P.; Burke, K.; Ernzerhof, M. *Phys. Rev. Lett.* **1997**, *78*, 1396−1396.
(80) Zhao, Y.; Truhlar, D. G. *J. Phys. Chem. A* **2005**, *109*, 5656−5667.
(81) Perdew, J. P.; Ruzsinszky, A.; Csonka, G. I.; Constantin, L. A.; Sun, J. *Phys. Rev. Lett.* **2009**, *103*, 026403.
(82) Zhao, Y.; Truhlar, D. G. *J. Chem. Phys.* **2008**, *128*, 184109.
(83) Peverati, R.; Zhao, Y.; Truhlar, D. G. *J. Phys. Chem. Lett.* **2011**, *2*, 1991−1997.

(84) Peverati, R.; Truhlar, D. G. *J. Chem. Phys.* **2011**, *135*, 191102.
(85) Staroverov, V. N.; Scuseria, G. E.; Tao, J.; Perdew, J. P. *J. Chem. Phys.* **2003**, *119*, 12129−12137.
(86) Boese, A. D.; Handy, N. C. *J. Chem. Phys.* **2002**, *116*, 9559−9569.
(87) Chai, J.-D.; Head-Gordon, M. *J. Chem. Phys.* **2008**, *128*, 084106.
(88) Chai, J.-D.; Head-Gordon, M. *Phys. Chem. Chem. Phys.* **2008**, *10*, 6615−6620.